

PAPER • OPEN ACCESS

Local modes analysis of a rotating marine ship propeller with higher order harmonic elements

To cite this article: Chen Feng *et al* 2016 *J. Phys.: Conf. Ser.* **744** 012138

View the [article online](#) for updates and enhancements.

You may also like

- [Steering magnetic micropropellers along independent trajectories](#)
Peter J Vach, Stefan Klumpp and Damien Faivre
- [THE POPULATION OF PROPELLERS IN SATURN'S A RING](#)
Matthew S. Tiscareno, Joseph A. Burns, Matthew M. Hedman et al.
- [The effect of propeller cap angle and fin size of PBCF on propeller performance](#)
A Trimulyono, A B Jatmiko, I P Mulyatno et al.



ECS
The
Electrochemical
Society
Advancing solid state &
electrochemical science & technology

DISCOVER
how sustainability
intersects with
electrochemistry & solid
state science research

Local modes analysis of a rotating marine ship propeller with higher order harmonic elements

Chen Feng¹, Chen Yong¹, and Hua Hongxing¹

¹ Institute of Vibration, Shock and Noise, Shanghai Jiao Tong University, No. 800 Dongchuan Road, Shanghai 200240, China

e-mail: chenfeng_me@sjtu.edu.cn

Abstract. An annular harmonic finite element for the computation of the local modes of a pretwisted ship propeller is developed. The elements take into account both the gyroscopic effect and centrifugal stiffening of the propeller blades. The displacement field is expressed by a truncated Fourier series along the angle and by polynomial shape functions in the radial direction. As an example, the dynamic behaviour, i.e. the nature frequency and local modes, of a ship propeller is studied, and compared with ANSYS, both of which have good consistency.

1. Introduction

Ship propeller shaft can be modelled as composed by a shaft and array of blades. In elementary rotordynamics, the propeller is assumed to be rigid body, contributing to the inertia of the rotor but not to its compliance, or simplified modelling the propeller as a modal mass and stiffness system attached to the shaft [1]. While sometimes, the dynamics behaviour of the blades influences the whole system [2], possibly giving way to dangerous phenomenon [3], or exciting the high frequency vibration of the shafts and acoustic emission of the ship [4].

The dynamics of an array of blades can be studied without any problem by using any commercial FEM code, which is quite time consuming. If no account is taken for its rotation, the sacrifice of computational time is acceptable, but things become more complex when gyroscopic and centrifugal stiffening effects due to rotation must be considered [5]. Even in some cases, the centrifugal softening effect can be found in classical finite element rotordynamics, which exists in high speed rotating, causes some of the natural frequencies to vanish, which leading to a sort of elastic instability [6].

Some improvements are made to overcome these defects. Ruzicka [7] demonstrated that shortcomings exist when performing modal reduction for rotor blades using classical, displacement-based finite elements and mixed finite element was instead in such procedure. Carrera [8, 9] defined a unified formulation to perform free-vibrational analyses of the rotating structures, which offers a procedure to obtain refined structural theories that account for variable kinematic description. A rotor with deformable disk and array of blades is considered and the results show the convenience of using refined models. Sun [10] developed a novel dynamic model for a pretwisted rotating compressor blade mounted at an arbitrary stagger angle using general shell theory. The model is validated by comparing to the literature and ANSYS results, showing good agreement. Genta [11, 12] used a complex coordinates approach to derive the equation of motion of disc and array of blades elements that takes into account the blades' stagger angle, but considered only the zero and first harmonic modes that are coupled with those of the rotor as a whole.

The higher order harmonic modes of the propeller blades are important for they can be excited at a resonance, which cause the high acoustic emission of the ship, even compromise the safety of the rotor system. The aim of this paper is to develop a generalized higher order harmonic finite element



formulation taking into accounts both the gyroscopic effect and centrifugal stiffening to study the flexural behaviour in the propeller blades. The propeller blades are assumed to be annular elements with displacements developed in Fourier series along the angle. The element matrices are programmed in a developed FEM code DYNROT [13,14]. As an example, the dynamic behaviour, i.e. the nature frequency and local modes at standstill and different rotating speed, of a ship propeller is studied, and compared with ANSYS.

2. General coordinates and element kinematics

The main assumptions to analyse the propeller blades are that all blades are equal, aligned along the radial direction and their shear centre coincides with the centre of mass of each section. The blades are modelled as Euler-Bernoulli beams, i.e. that shear deformations and rotational inertia of the cross-sections can be neglected.

A typical cross-section of a blade perpendicular to the radial direction is shown in Figure 1. G is the centre of mass of the section, u_1, u_2, u_3 are principal inertial axes while axes u, v and w lie along the radial, tangential and axial directions. The twist angle ψ can be varied along the blade radius r . The array is modelled as a 2D object, all its properties concentrated in the mid-plane of the blade.

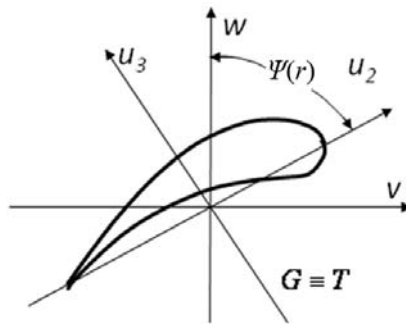


Figure 1. Cross section of blade.

Considering the reference frames showing in reference [12]. Let $u_j, v_j,$ and w_j be respectively the radial, tangential and axial displacement components of a point P_j of a section of the j th blade taken at a radius r . Define an inertial frame whose origin is O, \mathbf{P}_j is the coordinates in an inertial reference of point P expressed as

$$\overline{(\mathbf{P}_j - \mathbf{O})} = \overline{(\mathbf{C} - \mathbf{O})} + \prod_{k=1}^4 \mathbf{R}_k (\{r \ 0 \ 0\}^T + \{u_j \ v_j \ w_j\}^T), \tag{1}$$

where C and O are the coordinates of the shaft-blade attachment point and the inertial frame origin O, respectively. $\overline{\mathbf{P}_j - \mathbf{O}}$ is the displacement between the generic point P and the inertial frame origin O and $\overline{\mathbf{C} - \mathbf{O}}$ is the displacement between the shaft center C and the inertial frame origin O, \mathbf{R}_k are the rotation matrices as function of angle of the rigid body motion as reported in reference [12].

The zero and first order harmonics describes the torsional and axial vibration of the blades and the displacement field coupled to the flexural behavior of the shaft, in this paper the main purpose is to study the local modes of the blades. Thus rigid body motions are neglected and the deformation in the initial frame of point can be represented as the equation below.

$$\mathbf{P}_j = \begin{bmatrix} \cos \theta_j & -\sin \theta_j & 0 \\ \sin \theta_j & \cos \theta_j & 0 \\ 0 & 0 & 1 \end{bmatrix} \begin{Bmatrix} u_j \\ v_j \\ w_j \end{Bmatrix}, \tag{2}$$

3. Element shape functions

To define the shape functions approximating the deformations of the array of blades, the latter has been subdivided into annular elements. A non-dimensional radius χ , defined in the same way as seen for the disc element. A , I_2 and I_3 are the area of the cross section of each blade and its area moments of inertia about the principal inertia axis (2, 3 in Figure 1.) of the cross section. They are, together with angle ψ , linear functions of the nondimensional radius χ . The displacements u_j , v_j , w_j are then approximated by means of a truncated Fourier's series in the angular coordinate θ_j .

$$\begin{aligned} u_j(\chi, \theta_j, z, t) &= u_0 + \sum_{i=1}^n (u_{ic} \cos i\theta_j + u_{is} \sin i\theta_j), \\ v_j(\chi, \theta_j, z, t) &= v_0 + \sum_{i=1}^n (v_{ic} \cos i\theta_j + v_{is} \sin i\theta_j), \\ w_j(\chi, \theta_j, z, t) &= w_0 + \sum_{i=1}^n (w_{ic} \cos i\theta_j + w_{is} \sin i\theta_j). \end{aligned} \quad (3)$$

The coefficient of the various harmonics displacement $u_{ic,s}$ and $v_{ic,s}$ refer to the in-plane displacement while $w_{ic,s}$ are related to the out-of-plane displacement.

The dynamic behavior of the zero and first order harmonics of array of blades element have already been studied in reference [9], and in this paper only the second and higher order harmonics are dealt with. Due to the orthogonality of trigonometric functions, all harmonics contributions are decoupled with each other, and the use of truncated Fourier's series expansion will not lead to any major approximations. Here the terms for each higher order harmonics are listed.

$$[u, v, w]_j(\chi, \theta_j, t) = \sum_{i=2}^n ([u, v, w]_{ic} \cos i\theta_j + [u, v, w]_{is} \sin i\theta_j), \quad i \geq 2, \quad (4)$$

where the coefficient of the various harmonics displacement $u_{ic,s}$ and $v_{ic,s}$ refer to the in-plane displacement while $w_{ic,s}$ are related to the out-of-plane displacement, which can be approximated by shape functions \mathbf{n}_u , \mathbf{n}_v and \mathbf{n}_w , leading to

$$\begin{aligned} u_{ic}(\chi, t) &= \mathbf{n}_u(\chi) \mathbf{q}_{ux}(t), & u_{is}(\chi, t) &= \mathbf{n}_u(\chi) \mathbf{q}_{uy}(t), & v_{ic}(\chi, t) &= \mathbf{n}_v(\chi) \mathbf{q}_{vy}(t), \\ v_{is}(\chi, t) &= \mathbf{n}_v(\chi) \mathbf{q}_{vx}(t), & w_{ic}(\chi, t) &= \mathbf{n}_w(\chi) \mathbf{q}_{wx}(t), & w_{is}(\chi, t) &= \mathbf{n}_w(\chi) \mathbf{q}_{wy}(t). \end{aligned} \quad (5)$$

The in-plane circumferential and out-of-plane deflections of the blade element are coupled, and using shape functions of different order would lead to unacceptable approximations. Moreover, a shape function expressed by a cubic polynomial is what is commonly done in beam elements.

The generalized coordinates used to express the deflections of the array of blades coupled to the flexural behavior are:

$$\begin{aligned} \mathbf{q}_{ux}(t) &= \{u_{x1} \quad u_{x2}\}^T, & \mathbf{q}_{uy}(t) &= \{u_{y1} \quad u_{y2}\}^T, \\ \mathbf{q}_{vx}(t) &= -\{v_{x1} \quad \beta_{vx1} \quad v_{x2} \quad \beta_{vx2}\}^T, & \mathbf{q}_{vy}(t) &= \{v_{y1} \quad \beta_{vy1} \quad v_{y2} \quad \beta_{vy2}\}^T, \\ \mathbf{q}_{wx}(t) &= \{w_{x1} \quad \beta_{wx1} \quad w_{x2} \quad \beta_{wx2}\}^T, & \mathbf{q}_{wy}(t) &= -\{w_{y1} \quad \beta_{wy1} \quad w_{y2} \quad \beta_{wy2}\}^T. \end{aligned} \quad (6)$$

Since only second and higher order harmonics are dealt with, the terms for zero and first order harmonics are already eliminated in the above Equation (4).

4. Equations of motion of the element

4.1. Kinetic energy

Let $\mathbf{P}_{j,i}$ denoting the displacement of the center of mass of the j th blade at the radius r , relative to the inertial reference. The kinetic energy is

$$T_i = \frac{1}{2} \sum_{i=1}^N \int_{r_i}^{r_0} \rho A(r) \dot{\mathbf{P}}_{j,i}^T \dot{\mathbf{P}}_{j,i} dr, \quad (7)$$

where ρ is the density of the blades and $A(r)$ is the cross section of the blades at radius r .

In differentiating with respect to time, angle θ_j must be considered as a function of time. Owing to the orthogonality of the harmonic functions, a decoupling between the modes of the various orders occurs. The kinetic energy can be split between in-plane and out-of-plane contributions

$$T_i = T_{inp,i} + T_{outp,i} \tag{8}$$

The in-plane and out-of-plane contributions can be considered separately, therefore the in-plane and out-of-plane contributions to the kinetic energy is

$$\begin{aligned} T_{inp,i} = & \frac{1}{2} [\omega^2 (\mathbf{q}_{ux}^T \mathbf{m}_{inp1,i} \mathbf{q}_{ux} + \mathbf{q}_{uy}^T \mathbf{m}_{inp1,i} \mathbf{q}_{uy} + \mathbf{q}_{vx}^T \mathbf{m}_{inp2,i} \mathbf{q}_{vx} + \mathbf{q}_{vy}^T \mathbf{m}_{inp2,i} \mathbf{q}_{vy} - 2\mathbf{q}_{ux}^T \mathbf{m}_{inp3,i} \mathbf{q}_{vx} - 2\mathbf{q}_{uy}^T \mathbf{m}_{inp3,i} \mathbf{q}_{vy}) \\ & + \omega (\mathbf{q}_{uy}^T \mathbf{m}_{inp1,i} \dot{\mathbf{q}}_{ux} - \mathbf{q}_{vy}^T \mathbf{m}_{inp3,i} \dot{\mathbf{q}}_{ux} + \mathbf{q}_{ux}^T \mathbf{m}_{inp1,i} \dot{\mathbf{q}}_{uy} + \mathbf{q}_{vx}^T \mathbf{m}_{inp3,i} \dot{\mathbf{q}}_{uy} - \mathbf{q}_{uy}^T \mathbf{m}_{inp1,i} \dot{\mathbf{q}}_{vx} + \mathbf{q}_{vy}^T \mathbf{m}_{inp2,i} \dot{\mathbf{q}}_{vx} \\ & + \mathbf{q}_{ux}^T \mathbf{m}_{inp3,i} \dot{\mathbf{q}}_{vy} - \mathbf{q}_{vx}^T \mathbf{m}_{inp2,i} \dot{\mathbf{q}}_{vy}) + \frac{1}{2} (\dot{\mathbf{q}}_{ux}^T \mathbf{m}_{inp1,i} \dot{\mathbf{q}}_{ux} + \dot{\mathbf{q}}_{uy}^T \mathbf{m}_{inp1,i} \dot{\mathbf{q}}_{uy} + \dot{\mathbf{q}}_{vx}^T \mathbf{m}_{inp3,i} \dot{\mathbf{q}}_{vx} + \dot{\mathbf{q}}_{vy}^T \mathbf{m}_{inp3,i} \dot{\mathbf{q}}_{vy})]. \end{aligned} \tag{9}$$

$$T_{outp,i} = \frac{1}{2} [\omega^2 (\mathbf{q}_{wx}^T \mathbf{m}_{outp,i} \mathbf{q}_{wx} + \mathbf{q}_{wy}^T \mathbf{m}_{outp,i} \mathbf{q}_{wy}) + \omega (2\mathbf{q}_{wy}^T \mathbf{m}_{outp,i} \dot{\mathbf{q}}_{wx} - 2\mathbf{q}_{wx}^T \mathbf{m}_{outp,i} \dot{\mathbf{q}}_{wy}) + \dot{\mathbf{q}}_{wx}^T \mathbf{m}_{outp,i} \dot{\mathbf{q}}_{wx} + \dot{\mathbf{q}}_{wy}^T \mathbf{m}_{outp,i} \dot{\mathbf{q}}_{wy}].$$

Thus matrices $\mathbf{m}_{inp,i}$ and $\mathbf{m}_{outp,i}$ are given by integrals

$$\begin{aligned} \mathbf{m}_{inp1,i} &= \frac{N}{2} \int_{r_i}^{r_0} \rho A \mathbf{n}_u^T \mathbf{n}_u dr, & \mathbf{m}_{inp2,i} &= \frac{N}{2} \int_{r_i}^{r_0} \rho A \mathbf{n}_v^T \mathbf{n}_v dr, \\ \mathbf{m}_{inp3,i} &= \frac{N}{2} \int_{r_i}^{r_0} \rho A \mathbf{n}_u^T \mathbf{n}_v dr, & \mathbf{m}_{outp,i} &= \frac{N}{2} \int_{r_i}^{r_0} \rho A \mathbf{n}_w^T \mathbf{n}_w dr. \end{aligned} \tag{10}$$

4.2. Potential energy

According to reference [11], contributions to the potential energy due both to the elastic strain-stress natural of the material ($U_{e,i}$) and to the geometric effect ($U_{g,i}$) have been considered as

$$U_i = U_{e,i} + U_{g,i}. \tag{11}$$

Shear deformation in the blade is neglected, since each single blade is modeled as an Euler-Bernoulli's beam. The elastic energy is thus related to the radial extension and flexural deflections

$$U_{e,i} = \frac{1}{2} \sum_{j=1}^N \int_{r_i}^{r_0} E \left[\frac{A}{\Delta r^2} (s'_{1,i})^2 + \frac{1}{\Delta r^4} (I_2 (s'_{2,i})^2 + I_3 (s'_{3,i})^2) \right] dr. \tag{12}$$

The prime indicates the partial derivative relative to the radial coordinates r and E is the Young's modulus. The displacements s along the inertial axes is linked to the axial, tangential and radial directions by angle ψ , which is a function of the radial coordinate only

$$s_{1,i} = u_{j,i}, \quad s_{2,i} = v_{j,i} \cos \psi + w_{j,i} \sin \psi, \quad s_{3,i} = w_{j,i} \cos \psi - v_{j,i} \sin \psi. \tag{13}$$

Therefore, the contributions to the elastic potential energy are expressed in terms of element generalized coordinates as

$$\begin{aligned} U_{einp,i} &= \frac{1}{2} (\mathbf{q}_{ux}^T \mathbf{k}_{einp1,i} \mathbf{q}_{ux} + \mathbf{q}_{uy}^T \mathbf{k}_{einp1,i} \mathbf{q}_{uy} + \mathbf{q}_{vx}^T \mathbf{k}_{einp2,i} \mathbf{q}_{vx} + \mathbf{q}_{vy}^T \mathbf{k}_{einp2,i} \mathbf{q}_{vy}), \\ U_{eoutp,i} &= \frac{1}{2} (\mathbf{q}_{wx}^T \mathbf{k}_{eoutp,i} \mathbf{q}_{wx} + \mathbf{q}_{wy}^T \mathbf{k}_{eoutp,i} \mathbf{q}_{wy}). \end{aligned} \tag{14}$$

The stiffness matrices are obtained from the shape functions by the following integrals

$$\begin{aligned} \mathbf{k}_{einp1,i} &= \frac{N}{2\Delta r^2} \int_{r_i}^{r_0} E A \mathbf{n}'_u{}^T \mathbf{n}'_u dr, \\ \mathbf{k}_{einp2,i} &= \frac{N}{2\Delta r^4} \int_{r_i}^{r_0} E I_w \mathbf{n}''_v{}^T \mathbf{n}''_v dr, \\ \mathbf{k}_{eoutp,i} &= \frac{N}{2\Delta r^4} \int_{r_i}^{r_0} E I_v \mathbf{n}''_w{}^T \mathbf{n}''_w dr, \end{aligned} \tag{15}$$

where I_v and I_w are the area moments of inertia of the cross section in circumferential and axial direction v and w in Figure. 1.

The geometric potential energy is caused by the centrifugal forces $F_{r,i}$. Assuming that the blades are free to expand radially at its tip, the thermal effect do not induce any radial load along the axis of blades and force F_r can be expressed as

$$F_{r,i} = \omega^2 \int_r^{r_0} \rho A r dr. \tag{16}$$

And the geometric contribution to the potential energy can be split into two independent contributions and can be express as

$$U_{g,i} = U_{ginp,i} + U_{goutp,i} = \frac{1}{2\Delta r^2} \sum_{i=1}^N \int_{r_i}^{r_0} F_{r,i}(r) [v_{j,i}^2 + w_{j,i}^2] dr. \tag{17}$$

Integrating the equations, the geometric potential energy is

$$U_{ginp,i} = \frac{1}{2} (\mathbf{q}_{vx}^T \mathbf{k}_{ginp\omega,i} \mathbf{q}_{vx} + \mathbf{q}_{vy}^T \mathbf{k}_{ginp\omega,i} \mathbf{q}_{vy}),$$

$$U_{goutp,i} = \frac{1}{2} (\mathbf{q}_{wx}^T \mathbf{k}_{goutp\omega,i} \mathbf{q}_{wx} + \mathbf{q}_{wy}^T \mathbf{k}_{goutp\omega,i} \mathbf{q}_{wy}). \tag{18}$$

The stiffness matrices are given by the integrals of the shape functions

$$\mathbf{k}_{ginp\omega,i} = \frac{N}{\Delta r^2} \int_{r_i}^{r_0} P_{r\omega} \mathbf{n}'_v{}^T \mathbf{n}'_v dr,$$

$$\mathbf{k}_{goutp\omega,i} = \frac{N}{\Delta r^2} \int_{r_i}^{r_0} P_{r\omega} \mathbf{n}'_w{}^T \mathbf{n}'_w dr. \tag{19}$$

4.3. Element matrices

Higher order harmonics are uncoupled from the flexural behavior of rotor. If no external force acts on the element, the equations of motion for the higher order harmonics of the array of blades can be expressed as

$$\mathbf{M}_{inp,i} \ddot{\mathbf{Q}}_{inp,i} - i\omega \mathbf{G}_{inp,i} \dot{\mathbf{Q}}_{inp,i} + (\mathbf{K}_{inp,i} + \omega^2 \mathbf{K}_{\omega inp,i} - \omega^2 \mathbf{M}_{niinp,i}) \mathbf{Q}_{inp,i} = \mathbf{0},$$

$$\mathbf{M}_{outp,i} \ddot{\mathbf{Q}}_{outp,i} - i\omega \mathbf{G}_{outp,i} \dot{\mathbf{Q}}_{outp,i} + (\mathbf{K}_{outp,i} + \omega^2 \mathbf{K}_{\omega outp,i} - \omega^2 \mathbf{M}_{nioutp,i}) \mathbf{Q}_{outp,i} = \mathbf{0}, \tag{20}$$

The in-plane and out-of-plane coordinates can be assembled in vectors as

$$\mathbf{Q}_{inp,i} = \begin{Bmatrix} X_0 + iY_0 \\ \mathbf{q}_{ux} + i\mathbf{q}_{uy} \\ \mathbf{q}_{vx} + i\mathbf{q}_{vy} \end{Bmatrix}_{(7 \times 1)}, \quad \mathbf{Q}_{outp,i} = \begin{Bmatrix} \phi_{y0} - i\phi_{x0} \\ \mathbf{q}_{wx} + i\mathbf{q}_{wy} \end{Bmatrix}_{(5 \times 1)}. \tag{21}$$

The element mass, gyroscopic, centrifugal and thermal stiffening and stiffness matrices are obtained by using Lagrange's equations

$$\mathbf{M}_{inp,i} = \begin{bmatrix} 0 & 0 & 0 \\ 0 & \mathbf{m}_{inp1,i} & 0 \\ 0 & 0 & \mathbf{m}_{inp2,i} \end{bmatrix}, \quad \mathbf{M}_{outp,i} = \begin{bmatrix} 0 & 0 \\ 0 & \mathbf{m}_{outp,i} \end{bmatrix},$$

$$\mathbf{G}_{inp,i} = 2i \begin{bmatrix} 0 & 0 & 0 \\ 0 & \mathbf{m}_{inp1,i} & -\mathbf{m}_{inp3,i} \\ 0 & -\mathbf{m}_{inp3,i} & \mathbf{m}_{inp2,i} \end{bmatrix}, \quad \mathbf{M}_{niinp,i} = 2i^2 \begin{bmatrix} 0 & 0 & 0 \\ 0 & \mathbf{m}_{inp1,i} & -\mathbf{m}_{inp3,i} \\ 0 & -\mathbf{m}_{inp3,i} & \mathbf{m}_{inp2,i} \end{bmatrix}, \tag{22}$$

$$\mathbf{G}_{outp,i} = 2i \begin{bmatrix} 0 & 0 \\ 0 & \mathbf{m}_{outp,i} \end{bmatrix}, \quad \mathbf{M}_{nioutp,i} = i^2 \begin{bmatrix} 0 & 0 \\ 0 & \mathbf{m}_{outp,i} \end{bmatrix}.$$

The stresses in the radial and tangential directions can be computed from centrifugal and thermal loading. The stiffness matrices can be written as

$$\mathbf{K}_{inp,i} = \begin{bmatrix} 0 & 0 & 0 \\ 0 & \mathbf{k}_{einp1,i} & 0 \\ 0 & 0 & \mathbf{k}_{einp2,i} \end{bmatrix}, \quad \mathbf{K}_{\omega inp,i} = \begin{bmatrix} 0 & 0 & 0 \\ 0 & 0 & 0 \\ 0 & 0 & \mathbf{k}_{ginp\omega,i} \end{bmatrix}, \quad (23)$$

$$\mathbf{K}_{outp,i} = \begin{bmatrix} 0 & 0 \\ 0 & \mathbf{k}_{eoutp,i} \end{bmatrix}, \quad \mathbf{K}_{\omega outp,i} = \begin{bmatrix} 0 & 0 \\ 0 & \mathbf{k}_{goutp\omega,i} \end{bmatrix}.$$

As already mentioned in disc element matrices, rigid body displacements X_0+iY_0 and $\Phi_{y0}-i\Phi_{x0}$ are the rigid body motions of the array of blades. For second and higher order harmonics array of blades element, they should not be considered.

5. Example

5.1. Analyzed model

A ship propeller with six blades is studied here, the material and key stats of the propeller shaft are listed in Table 1 and Table 2. The propeller is modeled with commercial CAD/CAE software Solidworks as shown in Figure 2.

Table 1. Propeller shaft material property.

	Material	Young's Modulus (Gpa)	Density (kg/m ³)
Propeller	Ni-Al-Bronze Cu ₃	1.86	7590
Shaft	Steel	2.05	7850

Table 2. Key stats of the propeller.

No. Blades	6	Inner Radius	0.245m	Outer Radius	2.35m
Expanded Area Ratio	0.72	Pretwist Angle	30°	Mean Spacing	1.86m
Each Blade Mass	110kg	Blade Moment	40.6kg.m ³		

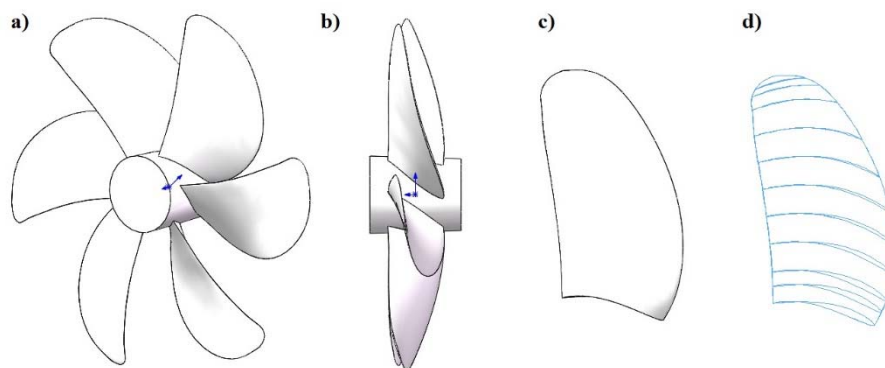


Figure 2. Ship propeller CAD/CAE model. a) Isometric view; b) Side view; c) blade model; d) cross sections and splines of a single blade.

Since the number of blades are even and the geometry of the blades are the same, the array is axisymmetric and ten higher order harmonic blade elements are used to model the propeller array of blades. For each blade element, the geometric centre, the moment of inertia and the twist angle ψ of all the cross sections of the blades are needed as shown in Figure 2d). Some of the cross sections along the non-dimensional radius χ are extracted and plotted, while the propeller array of blade high order harmonic finite element model (DYNROT model) are shown in Figure 3.

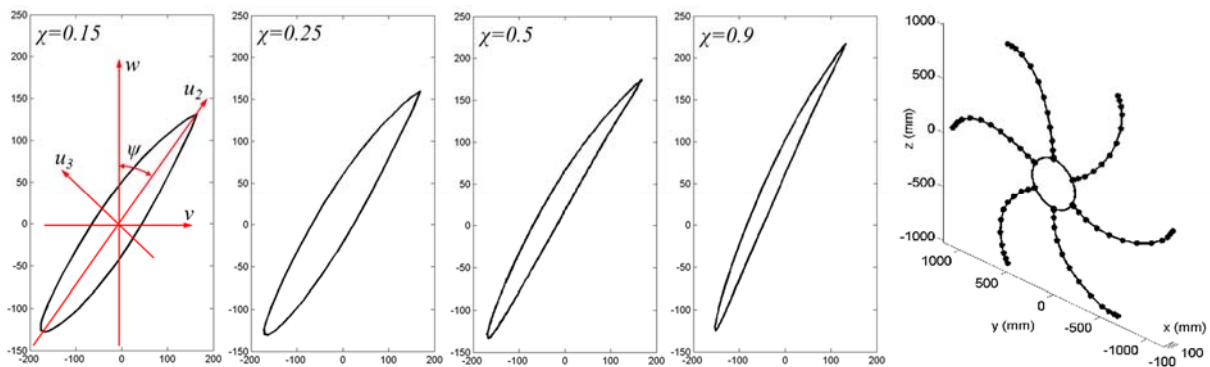


Figure 3. Some of the cross sections along the radius (non-dimensional radii $\chi=0.15, 0.25, 0.5, 0.9$) and propeller DYNROT model.

5.2. Local modes of the propeller at standstill

In this example, ANSYS is used to compute and compare the dynamics of the propeller. A series model with different mesh density is first structured to find the appropriate element number for the analyzing of propeller nature frequency and local modes of blades. The smart size mesh control tool integrated in ANSYS is used, the element number are varied from 8105 to 530715 (Smart size form Coarse 10 to Fine 1), the first four order nature frequencies related to the local modes of the propeller blades at standstill are compared in Figure 4. It is clear that with the increasing of element number, the nature frequencies approaching to a constant value. Since if the smart size is smaller than 6, the frequencies tend to be stable, while the element number increases dramatically, the smart size 5 is chosen for the following studying, i.e. 47473 ten node tet-element Solid 187 is used for the ANSYS propeller model.

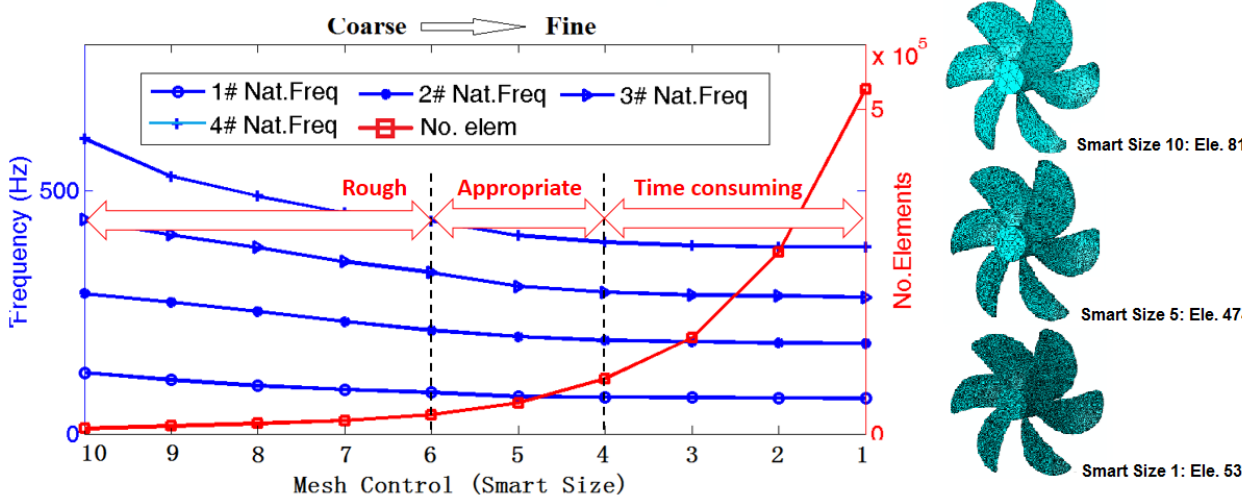
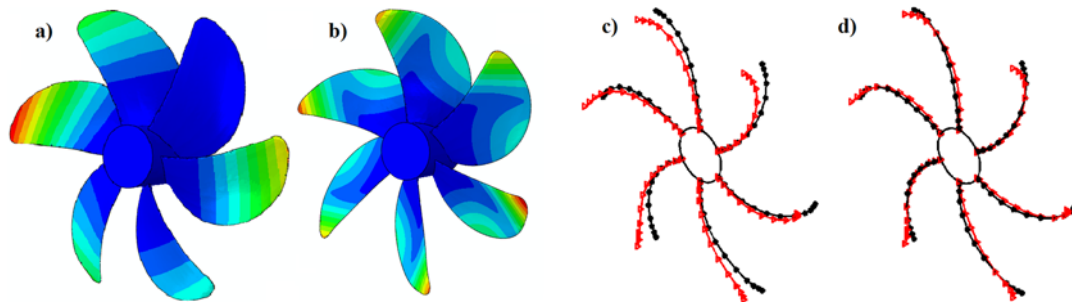


Figure 4. Compare of the nature frequencies and the number of elements with different mesh density.

As mentioned, ten higher order harmonic array of blades elements are used for the dynamic studying of the propeller blades. The computation is performed both by using all generalized coordinates and using Guyan reduction. Only the first four natural frequencies for the 2nd order harmonics at standstill are computed and compared with ANSYS as reported in Table 3. The first two local mode shapes for the 2nd order harmonics element and ANSYS model are compared in Figure 5.

Table 3. Propeller array of blades: comparison between the first four order natural frequencies for the 2nd order harmonics (local modes), $\omega=0$.

2 nd order harmonics array of blades					
Freq. (Hz)	No red.	Guyan red.	ANSYS	Min Error (%)	Max Error (%)
#1 mode	71.19	70.06	76.271	6.66	8.14
#2 mode	182.47	180.26	199.19	8.39	9.50
#3 mode	271.42	269.25	302.80	10.36	11.07
#4 mode	357.26	355.14	406.97	12.21	12.74

**Figure 5.** First two order local modes of 2nd order harmonics of ANSYS and DYNROT models, $\omega=0$; (a), (b): first-, second -order modes of ANSYS model; (c), (d) first-, second -order modes of DYNROT model; solid black line with *: un-deformed blades; solid red line with *: deformed blades.

From all the data above it follows that whatever the reduction method is used or not, the frequencies for the 2nd order harmonics fits well with the maximum error no more than 13%. It is also noticed that the modes for higher order harmonics of DYNROT model are in good agreement with that of ANSYS.

5.3. Local modes of the rotating propeller

When considering rotation, DYNROT model still agrees with ANSYS model if the gyroscopic effect is neglected. This means that in both models only centrifugal stiffening is taken into consideration. If all the contributions in DYNROT model are accounted for, ANSYS code underestimates the whirl frequency of forward modes, and this error increases with increasing speed. The comparison of the 1st nature frequency of the 2nd order harmonics at different rotating speed are plotted in Figure. 6. But as for ship propellers, generally the rotating speed is lower than 10Hz, which means the centrifugal stiffening and gyroscopic effect does not highly affect the rotating nature frequency of the propeller.

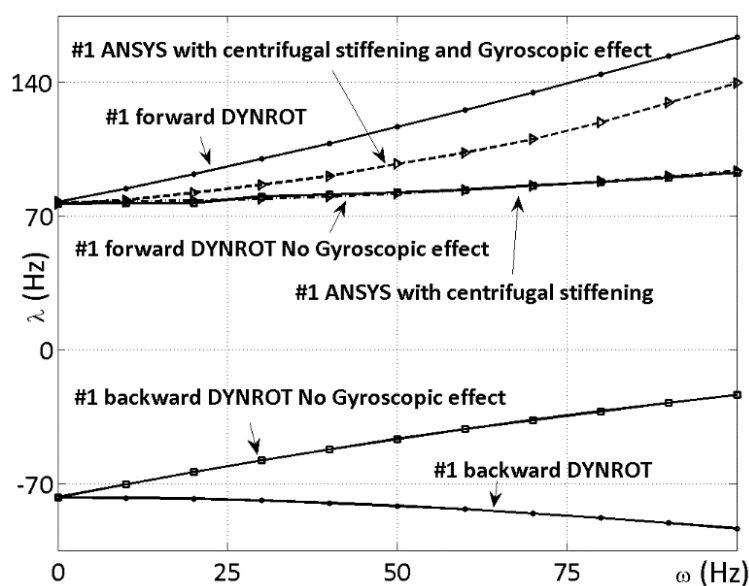


Figure 6. First forward and backward frequencies as functions of the speed for the propeller array of blades in DYNROT and ANSYS model.

6. Conclusion

A finite elements aimed at modeling the propeller blades for the study of the flexural behavior have been developed. The displacement field within the array of blades are approximated by trigonometrical expansion along the tangential direction and a polynomial expansion along the radius. Only the second and higher order harmonics have been taken into account as they are uncoupled from the dynamic behavior of the rotor.

The formulation for the element have been obtained using complex coordinates following a Lagrangian approach which accounts for gyroscopic effects and stress stiffening. The elements have been implemented in the existing FEM code DYNROT.

An example has been carried out to verify the accuracy of the element. The mesh density is first studied with ANSYS, the natural frequencies related to the local modes of the propeller blades at standstill and different rotating speed are compared with ANSYS and 2nd order harmonic model. The results show the element performs with a good accuracy, even when using a small number of degrees of freedom.

7. Acknowledgements

The authors would like to thank the NSFC for financially supporting this research under the contract No. 51405292.

8. References

- [1] ZG Zhang, F Chen, ZY Zhang and HX Hua 2013 Vibration Analysis of a Propeller-shaft System with Friction-induced Self-excited Oscillations *20th International Congress on Sound and Vibration* Bangkok Thailand.
- [2] P J Magari, L A Shultz and V R Murthy 1988 Dynamics of helicopter rotor blades *Computer and Structure* **29** 763-782.
- [3] G Genta On the stability of rotating blade arrays 2004 *Journal of Sound and Vibration* **273** 805-836.
- [4] ZG Zhang, F Chen, ZY Zhang and HX Hua 2014 Analysis of friction-induced vibration in a propeller-shaft system with consideration of bearing-shaft friction *Proceedings of the Institution of Mechanical Engineers, Part C: Journal of Mechanical Engineering Science* **228**(8) 1311-1328.

- [5] A Leissa 1981 Vibration aspects of rotating turbo machinery blades *Applied Mechanics Review* **34** 629-635.
- [6] G Genta and M Silvagni 2014 On Centrifugal Softening in Finite Element Method Rotordynamics *Journal of Applied Mechanics* **81** No. 011001.
- [7] G C Ruzicka and D H Hodges 2001 Application of the Mixed Finite-Element Method to Rotor Blade Modal Reduction *Mathematical and Computer Modeling* **33** 1177-1202.
- [8] E Carrera, E M Filippi and E Zappino 2013 Analysis of Rotor Dynamic by One-Dimensional Variable Kinematic Theories *Journal of Engineering for Gas Turbines and Power* **135** No.092501.
- [9] E Carrera, E M Filippi and E Zappino 2013 Free Vibration Analysis of Rotating Structure by One-Dimensional, Variable Kinematic Theories, *Proceedings of the ASME 2013 International Mechanical Engineering Congress and Exposition*, San Diego, California, USA.
- [10] Jia Sun, I L Arteaga and L Kari 2013 General shell model for a rotating pretwisted blade *Journal of Sound and Vibration* **332** 5804–5820.
- [11] G Genta and A Tonoli 1996 A harmonic finite element for the analysis of flexural, torsional and axial rotordynamic behavior of discs *Journal of Sound and Vibration* **196** 19-43.
- [12] G Genta and A Tonoli 1997 A harmonic finite element for the analysis of flexural, torsional and axial rotordynamic behavior of blade arrays *Journal of Sound and Vibration* **207** 693-720.
- [13] G Genta, C Delprete and D Bassini 1996 DYNROT: a finite element code for rotordynamic analysis based on complex co-ordinates *Engineering Computations* **13** 86-109.
- [14] G Genta, F Chen and A Tonoli 2010 Dynamics behavior of rotating bladed discs: A finite element formulation for the study of second and higher order harmonics *Journal of Sound and Vibration* **329** 5289–5306.